Examining the Performance of Single-Slope Desalination Using SS302 Hollow Circular Fin Absorbers at Varying Heights

Syamsul Hadi[1*] , Muhamad Dwi Septiyanto[1,2], Aristya Naziha Parahita[1], Indri Yaningsih[1] , Eko Prasetya Budiana[1]

[1] Mechanical Engineering, Faculty of Engineering, Universitas Sebelas Maret, Surakarta 57126, Indonesia
[2] Master Program of Mechanical Engineering, Faculty of Engineering, Universitas Sebelas Maret, Surakarta 57126, Indonesia

Corresponding Author Email: syamsulhadi@ft.uns.ac.id

ABSTRACT

The application of fins as a solar heat absorber on solar still desalination has gained attention to enhance productivity, efficiency and cut heat losses. Considering the effectiveness of fin configuration, it is still the focus of development by many researchers. To determine the optimum height configuration, this study conducted an experimental analysis of hollow circular fin (HCF) height as variation during the day testing under the Kentingan Sebelas Maret University climates. Moreover, the hollow circular fin is constructed utilizing the SS302 material. The variation used is conventional CS4, which incorporates the supplementary heights of 20 mm, 40 mm, and 60 mm for the hollow circular fins. Overall, the study has identified a consistent decrease in efficiency as the HCF increases, with efficiency gains of 40.96%, 35.39%, and 29.16%. However, different circumstances yield favorable outcomes, exhibiting a notable improvement of 10.30% and 5.57% in enhanced efficiency for 20 mm and 40 HCF, respectively, compared to conventional solar stills against the analysis that can evaluate the energy loss through the partition and solar still wall. A correlation analysis was conducted using both experimental productivity data and analysis prediction data to ensure that this experiment analysis yielded excellent results compared to others.

1. INTRODUCTION

The Earth's structure is predominantly composed of water, which comprises approximately 97% of its volume. Nevertheless, a high percentage of water cannot all be consumed by humans because of saline water (94%) and polar ice (2%), while only 1% is acceptable for human daily consumption [1]. Both the rapid growth in the human population and the advent of the Industrial Revolution have significantly affected the need for freshwater consumption [2]. Interestingly, the development of seawater purification technology drew the interest of researchers for further studies. The purification process of seawater into freshwater is also known as the seawater desalination process. Over the past six decades, solar energy-based seawater desalination has garnered significant interest from researchers. During World War II in 1940, the military required the use of solar energy to desalinate seawater [3, 4]. Solar still consists of active and passive solar systems, which share the common principle of evaporating seawater and subsequently condensing the vapor to produce distilled water that is safe for consumption. Furthermore, active solar still specifically pertains to the salination process, which involves the periodic filling of a chamber using pumps and other mechanical devices. On the other hand, passive solar still refers to a salination system that does not rely on a conventional filling system [5].

CS4 was a type of distillation that was suitable for both small and large-scale production, with an estimated productivity of approximately 1.36 liters per day. This device operates by evaporating water in a sealed chamber and subsequently condensing the resulting vapor into freshwater captured by a partition glass and accumulated in a container [6, 7]. CS4-based desalination has been claimed to purify seawater with a high salt content of up to 104 ppm [8]. This considerable purification process offered a significant opportunity for the advancement of CS4 technology. However, it was necessary to maintain the delicate equilibrium between the extensive results and the overall energy input into the solar still system, considering the heat loss. The right and bottom side walls facilitate the transmission of heat dissipation during CS4's salination process [9]. Figure 1 depicts the percentage distribution of the heat energy that enters the chamber of the solar still.

Numerous investigations have been undertaken on the shape of the fin configuration in various forms. Rajaseenivasan et al. [10] conducted a study that examined the comparison of productivity produced by a single slope with variations in square and circular fins. The results showed that the circular fin configuration demonstrated a better-distilled water output. In addition, Jani et al.'s study employed a square fin configuration with a circular fin on a double-slope solar still with varying submerged depths of 10 mm, 20 mm, and 30 mm. Implementing circular fin height on the double-slope led to a substantial rise in productivity, rising by 54.22%, 38.49%,

and 43.86% at different depths below the surface [11]. Research on the various aspects of the fin configuration as an absorber continues to be carried out, ranging from the number of fins utilized in the chamber [12], fin orientation [13], inclined fin [14], and shape of the fin configuration (e.g., rectangular [15], hollow circular [16], hollow cylindrical, and square fin [17]). Table 1 provides a concise summary of the utilization of fin absorbers in desalination systems.

Several studies have altered the sea water level within the solar still chamber to identify the balanced mass capacity needed to produce optimum solar still productivity [11, 18]. The results generally indicated that as the water level rises, there is a corresponding drop in the productivity of the solar still. This is because the greater water mass requires a larger amount of energy to evaporate the seawater, resulting in a steady decrease in the rate of condensation. In this experimental analysis study, the water height and water mass remained constant while the height of the hollow circular fin (HCF) was varied. Prior studies have explored differences in fin height using other types of fins, namely FLBS and tube iron

fins [19, 20]. Both experiments assessed the performance of the fin in the solar still, but they did not determine how energy was dissipated through the wall and glass partition. The research lacked investigation of the variation in fin types, namely the utilization of hollow circular fins in a single-slope solar still. The second was employing statistical analysis to compare predicted and experimental productivity data. This was done to demonstrate that it is valid to compare the results using a normal distribution, taking into account the variations in solar radiation intensity received daily.

Based on the literature, three types of energy are reflected from partition glass, seawater, and absorbers into the environment through partition glass [21]. The limitation of this study was that dissipated energy resulting from the interaction between an unexposed seawater HCF and reflected energy from seawater to the environment was only accounted for by total energy losses through the partition glass ($Q_{T,glass}$). In addition, the energy dissipated through the side and bottom walls is represented by $Q_w + Q_b$.
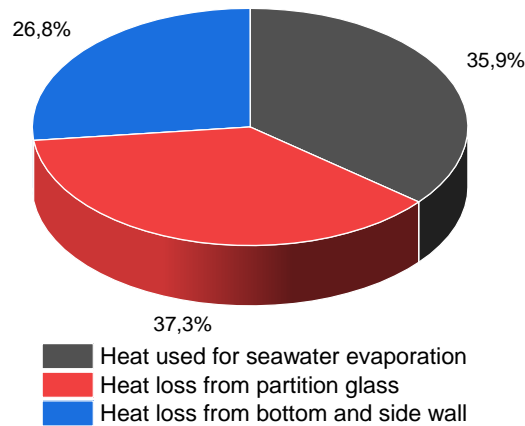

Figure 1. The heat percentage distribution on solar still

Table 1. The related study on the use of fin absorbers in desalination systems

Ref.	Topic	Solar Still	Results
[13]	Comparing the performance of different quantities of horizontal flat fins	Single-slope solar still	18.5% and 7% of productivity increased at n = 15 and n = 10 fins, respectively.
[12]	Comparing the performance of vertical hollow circular fins	Single-slope solar still	6.06% and 22.85% of productivity enhancement in n = 176 and n = 216, respectively.
[14]	Comparison of vertical and inclined fin absorbers	Tubular solar still	The vertical and inclined fin productivity increased by 18% and 27.6%, respectively, compared to conventional solar stills.
[19]	Comparison of iron fin spacing with additional variable height	Hemispherical solar still	The increase in fin quantity gradually increases efficiency and productivity, but at some point, it decreases their performance.
[10]	Performance comparison of circular and square fins	Active solar still	Both circular and square fins gained higher productivity with 26.3% and 36.7%, respectively.
[11]	Performance comparison of hollow circular and square fins	Double-Slope Solar Still	Both hollow circular and square fins enhanced the efficiency by 45.53% and 23.90%, respectively, compared to conventional solar stills.
[22]	Performance comparison of finned and corrugated fins	Single-slope solar still	Both finned and corrugated absorbers increase productivity by 21% and 40%, respectively.

2. MATERIAL AND METHOD

2.1 Experimental Set-up

A conventional single-slope solar still (CS4) was utilized in this study, as shown in Figure 2. We designed this model to

construct the testing chambers, which were equipped with stainless steel layers to serve as reflectors. The seawater within the system absorbs heat from the high levels of radiation, causing the temperature and moisture in the chamber to progressively rise. As discussed theoretically, natural convection occurs in the space between the inner glass and the

bottom chamber of the chamber. The elevated temperature of the seawater and variations in pressure facilitate the movement of the vapor into the upper chamber. When the surrounding air contacts the outer glass, the saturated vapor is condensed. The transition phase of water is enhanced by previous research, and the phenomenon of condensed water is also examined in terms of temperature disparities between the surrounding area and the system [23]. The specifications of the solar still used are as follows:

a) The partition glass is made of transparent glass measuring 5 mm in thickness and 71×95 mm in dimension, with a 25° inclination. The system transmits solar radiation to both the absorber plate and seawater while also collecting condensation water.

b) The solar still was adorned with black-painted stainless-steel reflectors. The chamber has the following dimensions: a length of 955 mm, a width of 735 mm, a back height of 405 mm, a front height of 86 mm, and a plate thickness of 3 mm.

c) The solar still's outer wall was constructed using plywood measuring 1361 mm in length, 765 mm in width, 8.6 mm in front height, and 405 mm in height at the back.
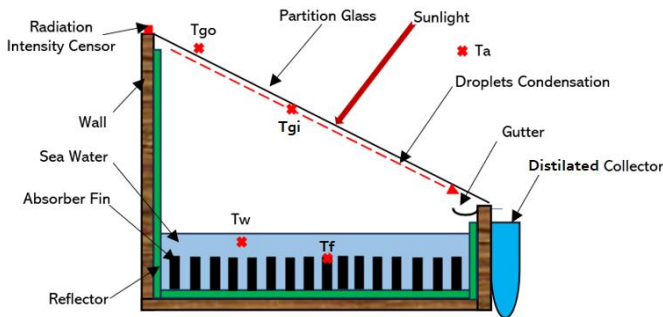

Figure 2. A schematic of the solar still used during the testing process with the detailed part and attached thermocouple censor

Figure 2 depicts the CS4 device, showing the fin positioned within the chamber and the placement of temperature sensors on the inner glass, outer glass, seawater, and fin. The used temperature recording device could measure temperatures ranging from -200°C to 200°C with an accuracy of 1°C. The temperature measurement process employed thermocouple sensors attached to various components of the CS4, as illustrated in Figure 2. A solar power meter measured the magnitude of solar radiation intensity throughout the testing period. The measurement of radiation intensity was conducted using a solar power meter of type SPM-1116SD, which has a range of 0-2000 W/m^2 and an accuracy of ±1 W/m^2.

2.2 Hollow circular fin configuration

A fin refers to a simple component employed in solar stills to enhance the surface area for heat absorption. Increasing the fin surface area enhances the transfer of heat through convection and increases the overall production, which is the main objective of the use of fins [24]. The utilization of fins in a conventional single basin solar still resulted in a gradual decrease in the time needed to preheat the chamber and evaporate the seawater. Both seawater and absorber temperatures progressively increased in a linearly proportional manner as the absorption area expanded. Given these circumstances, it has the potential to increase the disparity in

temperatures between the outer and inner glass, which is considered the primary cause of condensation [25]. Our study employed a hollow circular absorber fin made of SS304 series stainless steel. The fin consisted of a total of 117 pieces with three different heights, namely 20, 40, and 60 mm. The fin material had a thickness of 4 mm and a fin spacing of 57.50 mm. Detailed information on the hollow circular fin is depicted in Figure 3. Meanwhile, Table 2 presents detailed information about the HCF fin.
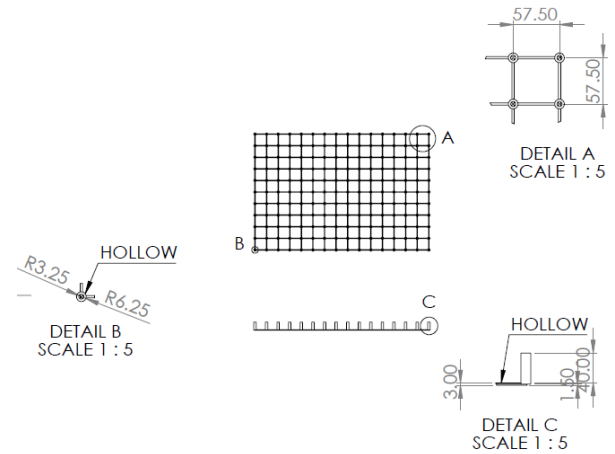

Figure 3. The detailed dimension HCF

Table 2. Properties of HCF

Parameter	Value
Thermal Conductivity	16.3 W/mK
Density	79.000 g/cm^3
Tensile Strength	620 MPa
Specific Heat	0
Transmissivity	500 J/kg·K

2.3 Testing procedure

This research was conducted on September 6, 11, 12, 13, and 15, 2022. Four different condition chambers were utilized and evaluated under the climatic conditions of Universitas Sebelas Maret, located in Kentingan, Surakarta. The operating hours were from 07.00 - 18.00 GMT+7. The conventional CS4 is referred to as Chamber 1, whereas CS4 with 20 mm HCF is referred to as Chamber 2, CS4 with 40 mm HCF is referred to as Chamber 3, and CS4 with 60 mm HCF is referred to as Chamber 4. All chambers underwent simultaneous testing until their productivity levels were nearly identical. The temperature is measured using a K-type thermocouple, and the sensors used for installation are shown in Figure 1. These sensors include seawater temperature (T_w), HCF (T_f), inner glass (T_{ig}), outer glass (T_{og}), and ambient (T_a). The data logger automatically captures data from all the thermocouples it is integrated into on an hourly basis. Figure 4 depicts the research flow chart in detail.

The saturated water vapor condensed on the partition glass, gathering in a gutter and entering the measuring cup. The hourly measurement of freshwater production was conducted until 18.00. A solar power meter demonstrated that solar radiation acted as the primary energy source for desalination. Similar to the other measured data, the radiation intensity data was collected hourly until the conclusion of the testing day. The last step involves scrutinizing the research data, with a particular emphasis on:

a) The effect of incorporating height variation in the HCF on the productivity and hourly rate of the solar still.
b) The effect of increasing the height of HCF on the energy balance of the system.
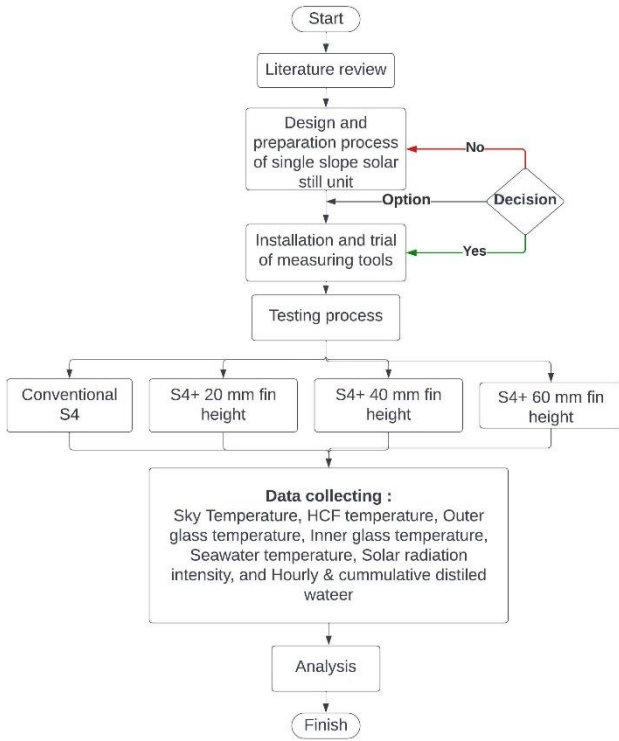c) The internal distribution temperature of every solar still chamber.

Figure 4. Experiment flowchart

2.4 Uncertainty analysis

The errors that arise throughout the process of experimental analysis encompass both bias errors (δb) and random errors (δr). This study examines the concepts of propagation error $\delta N = \sqrt{\delta b^2 + \delta r^2}$, temperature error (∂T), solar radiation intensity error (∂I_t), productivity error (∂M_w), and efficiency error $(\partial \eta)$. The bias error of the study refers to the level of accuracy of the measurement instrument, as represented by Table 3. The equations provided below depict the errors arising from this experimental analysis.

$$\partial T = \sqrt{\delta T_1 + \delta T_2 + \dots \delta T_n} \tag{1}$$

$$\partial I_t = \sqrt{\delta I_{t1} + \delta I_{t2} + \dots \delta I_{tn}} \tag{2}$$

$$\partial M_w = \sqrt{\delta M_{w1} + \delta M_{w1} + \dots \delta M_{wn}} \tag{3}$$

$$\partial h_{fg} = \sqrt{\left(\frac{\delta h_{fg}}{\delta T_w} \times \partial T_w\right)^2} \tag{4}$$

$$\partial \eta = \sqrt{\left(\frac{\partial \eta}{\partial M_w} \times \partial M_w\right)^2 + \left(\frac{\partial \eta}{\partial h_{fg}} \times \partial h_{fg}\right)^2 + \left(\frac{\partial \eta}{\partial I_t} \times \partial I_t\right)^2 + \left(\frac{\partial \eta}{\partial A} \times \partial A\right)^2} \tag{5}$$

The variables $\partial \eta$, $\partial T, \partial h_{fg}$, ∂I_t, and ∂M_w represent the overall error in efficiency, temperature, latent heat of evaporation, productivity, and absorber area, respectively. Afterward, the propagation error value for each measurement data within a single day is calculated using δT_1, δI_{t1}, δM_{w1}, and δh_{fg}. To strengthen the validity of the research findings, the productivity of solar stills per day in each chamber was assessed using the model equation derived from previous research [26]. Where n represents the amount of data, M_{pred} represents the analytical productivity data, and M_{exp} represents the experimental productivity data.

$$RMSE = \sqrt{\sum_{i=1}^{n} \frac{(M_{pred} - M_{exp})^2}{n}} \tag{6}$$

Table 3. Device specifications

Name	Uncertainty	Range
Lutron Solar Power Meter	± 10 W/m^2	0-2000
Thermocouple Censor	± 0.1°C	0-650°C
Pyrex Measurement Glass	± 1 mL	1-1000 mL

2.5 General equation

The absorber fin included during the research was a method to optimize the entering energy into the system [24, 27]. The term "entering energy" denotes the level of radiation intensity, which serves as the main factor contributing to increased production. The presence of the additional fin in the basin had a significant impact on temperature variations and the occurrence of natural convection. The effectiveness of various fin configurations was determined through additional calculations involving the input and utilization of energy [11, 17, 28]. To measure energy efficiency, one can determine the amount of energy that enters and is used by the system using the following equation [23, 29].

$$Qin = \tau \times I(t) \times A \tag{7}$$

$$Quse = \frac{m_{sw} \times h_{fg}}{t} + \frac{m_w \times c_{p\times}(T_f - T_i)}{t} \tag{8}$$

Qin and Quse represent energy units measured in watts (W), transmissivity is denoted by τ, and solar radiation intensity is represented by $I(t)$ (W/m^2), where A is the area of the glass partition (m^2), which serves as the entranced medium for sunlight, and m_{sw} and m_w refer to the mass of seawater in the chamber and the mass of CS4 productivity, respectively. Where h_{fg} represents the enthalpy gained, which is calculated using the following equation:

$$\begin{aligned} h_{fg} = 1000 \times (&2501.9 - 2.40706\, T_w \\ &+ 1.192217 \times 10^{-3} \times T_w^2 \\ &- 1.5863 \times 10^{-5} \times T_w^3) \end{aligned} \tag{9}$$

T_w denotes the seawater temperature within the basin during the testing process, while h_{fg} is measured in kJ/kg. Hence, the efficiency of the solar still may be determined using the equation provided below.

$$\eta_{passive} = \frac{\sum m_w \times h_{fg}}{\sum I(t)_s \, x \, A_s \times 3600} \tag{10}$$

With m_w as the mass of distilled water in kg. The solar still efficiency of the four chambers may be calculated. Figure 6 displays the data obtained from the measurement of solar radiation intensity during the testing process. The data intensities were averaged to calculate the entering energy into the solar still. Thus, based on the premise, it may be inferred that the solar's entering power remained constant. Figure 5 provides the entering and used energy in the solar still.

Chamber CS4 failed to fully absorb the energy received by the system during this experiment on seawater evaporation. The system released some energy into the surrounding environment through the glass barrier $Q_{T,glass}$, and the walls of the chamber. According to Sharshir et al., the energy released by the partition glass can take the form of radiation ($Q_{R,glass}$) or convection ($Q_{C,glass}$) [23].

$$Q_{R,glass} = h_{R,glass} \times (T_{og} - T_a) \quad (11)$$

$$Q_{C,glass} = h_{C,glass} \times (T_{og} - T_a) \quad (12)$$

With T_{og} as the measured temperature on the outside of the glass, T_a as the ambient temperature, and v as the wind speed. The values of the convection heat transfer coefficient ($h_{C,glass}$) and radiation ($h_{R,glass}$) can be calculated as follows:

$$h_{R,glass} = \varepsilon_g \sigma \left[\frac{(T_{og} + 273)^4 - (T_{Sky} + 273)^4}{T_{og} - T_a} \right] \quad (13)$$

$$h_{c,glass} = 2.8 + (3.0 \times v) \quad (14)$$

$$T_{Sky} = T_a - 6 \quad (15)$$

Subsequently, the heat losses via the partition glass can be represented as follows:

$$Q_{T,glass} = Q_{R,glass} + Q_{C,glass} \quad (16)$$

The heat propagation through the wall of the solar still was equal to the total of the heat propagation across the side and bottom walls. The transmission of heat from the seawater to the wall takes place through convective heat transfer Q_s, followed by convective heat transfer from the wall to the environment through conduction (Q_b) [23].

$$Q_w = h_w(T_{ch} - T_w) \quad (17)$$

$$Q_b = h_b(T_{ch} - T_a) \quad (18)$$

The temperature of the chamber wall was T_{ch}, whereas the temperature of the seawater was T_w. The relationship between the convective coefficient h_w and the conductive coefficient h_b can be used to describe the total bottom heat loss (C_b) released into the surroundings. The experiment chamber employs glass wall insulation to minimize heat transfer through the wall, hence decreasing the insulation's heat loss flow rate (L$_{insulation}$) and conductivity coefficient (K$_{insulation}$).

$$C_{bw} = \frac{h_w \times h_b}{h_w + h_b} \quad (19)$$

$$h_b = \left[\frac{L_{insulation}}{K_{insulation}} + \frac{1}{h_{R,wall}} \right]^{-1} \quad (20)$$

$$h_{R,wall} = 5.6 + (3.8 \times v) \quad (21)$$

Then $h_{R,wall}$ was the radiation coefficient from the wall to the surrounding environment. The total heat propagation coefficient of the system (C_T) is the sum of the total transfer coefficients from the side (C_{sw}) and bottom wall (C_{bw}) to the surroundings, as follows:

$$C_{sw} = \frac{A_{sw}}{A_{ch}} \times C_{bw} \quad (22)$$

$$C_T = C_{bw} + C_{sw} \quad (23)$$

The heat loss via the wall was calculated using the overall basin area (A$_{ch}$) and the side walls (A$_{sw}$). In this study, the sequential process of heat loss at the side wall involves convection from seawater to the wall, followed by conduction from the inner wall propagating through the insulation and surroundings, and ultimately, convection radiation from the outer surface of the chamber to the environment. The bottom wall experienced heat loss due to the transfer of heat through convection from the seawater to the wall, which was then followed by conduction.
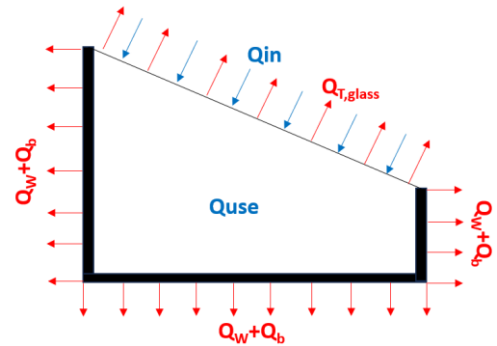

Figure 5. The schematic of system energy equilibrium

3. RESULT AND DISCUSSIONS

3.1 Relationship of radiation intensity with temperature in the chamber

Solar energy becomes the primary energy source driving the passive solar still. Due to these factors, the production of solar stills was greatly influenced by the radiation intensity during the testing period. In this study, the sun's motion appeared to be from east to west. Hence, the researchers strategically positioned the desalination device in the southern region to shield it from direct exposure to sunshine during the testing phase. The tests were conducted over five days, precisely on September 6, 11, 12, 13, and 15, 2022. Figure 6 depicts the level of solar intensity that was received during the testing period. In general, the intensity of solar radiation fluctuated. Wind speed and cloud conditions had a significant impact on the fluctuating radiation intensity [22]. The decision to compute the average of the accepted radiation intensity was made to streamline the energy calculation for these experiments. Moreover, the mean solar radiation intensity was measured at 6.406 W/m^2. Based on the R-square value of 0.875, the positive correlation is sufficiently significant, indicating that the performance data recorded in each chamber is comparable.
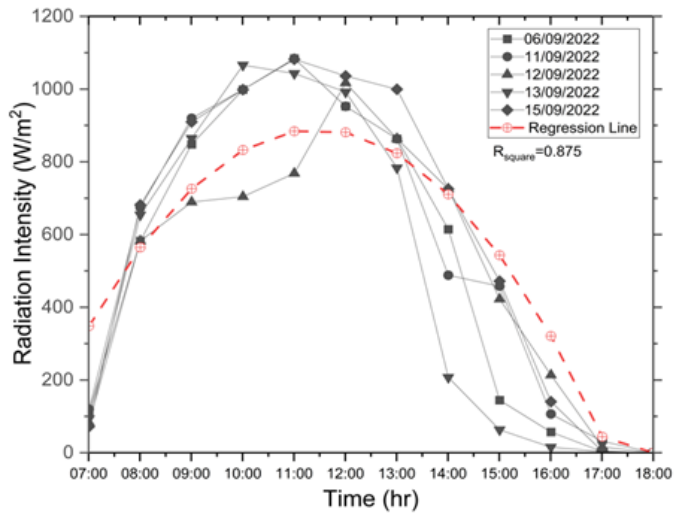
Figure 6. The plotted radiation intensity during the day testing

The system obtained its energy from solar radiation originating from chambers with varying heights of HCF. The incorporation of HCF led to distinct temperature plots for each chamber. The temperature change trends (T_f, T_w, T_{og}, and T_{ig}) exhibited a direct relationship with the amount of energy entering the system (Figure 6). Figure 7(a) illustrates a plot

displaying the temperature of seawater in the chamber. Furthermore, Figure 7(a) illustrates that T_w (pink line) in chamber 2 (20 mm HCF) consistently maintained the highest degree of dominance throughout the research day. The height of the HCF fin is directly proportional to the initial seawater level at the beginning of the experiment. This facilitates the most efficient absorption and usage of incoming energy to elevate the temperature of the seawater.

Figure 7(b) demonstrates that the average T_{ig} measured in Chamber 2 consistently exhibits lower values in comparison to the other chambers. The increased productivity of chamber 2 in this study, resulting in a greater amount of droplet film on the inner glass and a largely low-temperature plot, can account for these findings. According to prior research, the purpose of implementing the fin absorber is to ensure that the temperature decrease in the chamber remains consistent while the weather conditions vary throughout the study [30]. According to Figure 7(d), the fin temperature graphs for 60 mm and 40 mm HCF were greater than those for 20 mm HCF between 11.00. and 16.00. However, at 18.00, the temperature graphs of both chambers were lower than 20 mm HCF, indicating that chamber 2 has a higher likelihood of producing compared to the other chambers. The experimental data indicates that certain areas measuring 40 and 60 mm HCF, not exposed to saltwater, cause a temperature decrease. This allows the heat to rapidly dissipate between 07.00 and 12.00 through convection, transferring it to the glass partition and then dissipating into the environment.
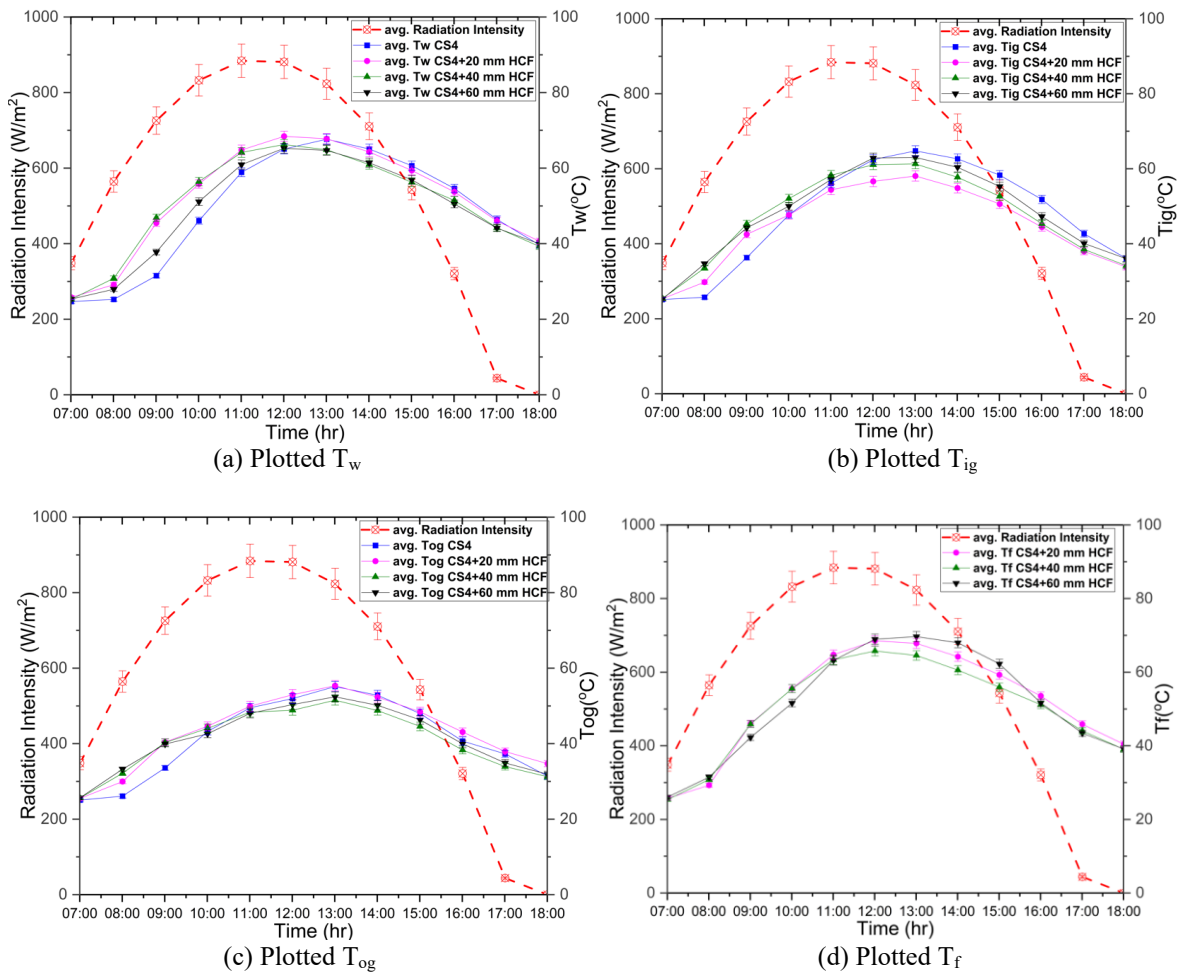

(a) Plotted T_w

(b) Plotted T_{ig}

(c) Plotted T_{og}

(d) Plotted T_f

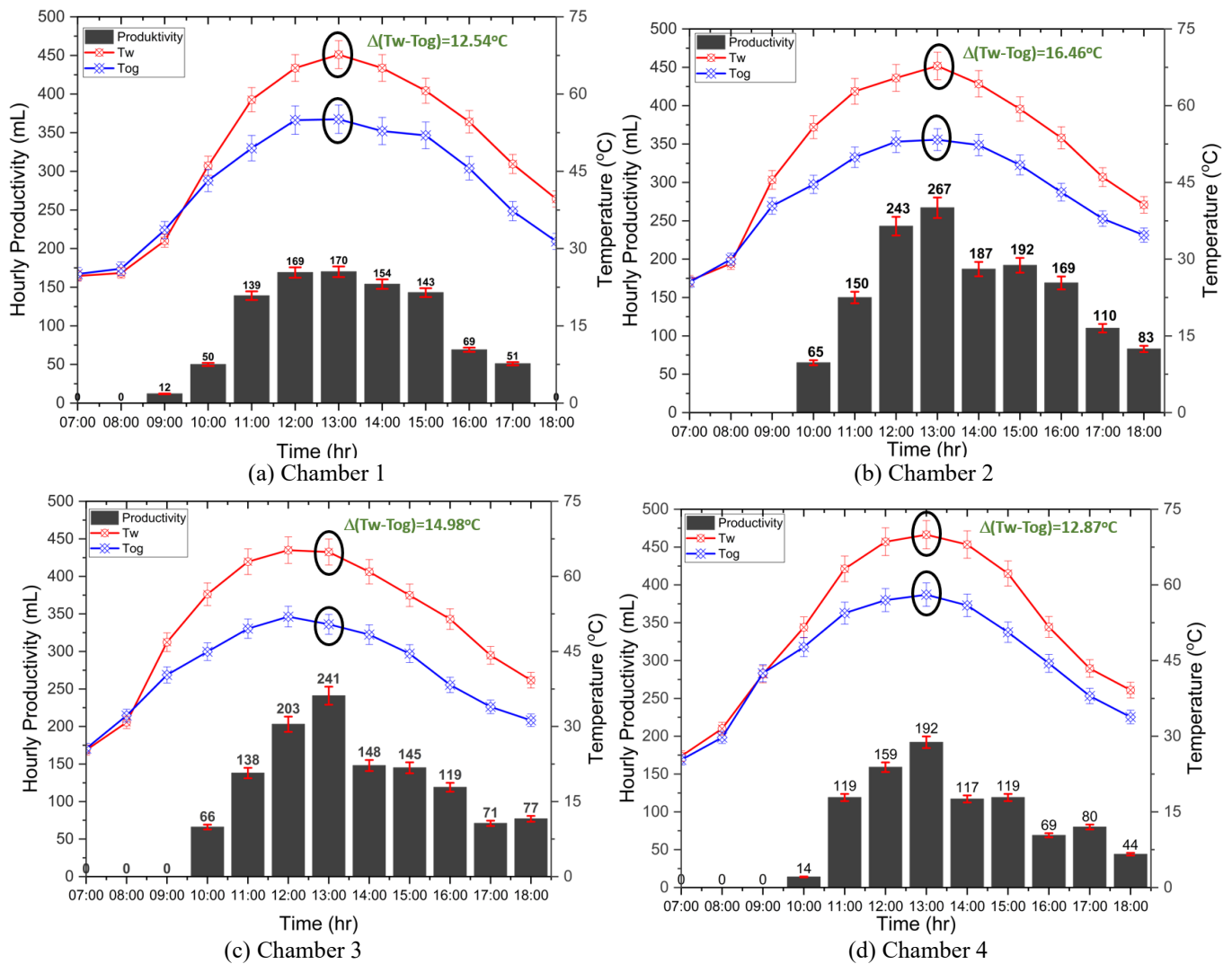**Figure 7.** The relationship between the plotted temperature and radiation intensity in each testing chamber

Figure 8. The relationship between the plotted (Δ(Tw-Tog)) and hourly productivity

3.2 Relationship of temperature differences with hourly productivity

Solar stills experienced substantial energy losses throughout the testing process. This supports the claim that the salination process still wastes more than 60% of the solar energy it receives [31]. To optimize the amount of energy absorbed, a variable absorber fin was added to enhance stability and regulate internal temperature. This adjustment aims to produce the most efficient evaporation process and minimize heat loss [32]. Maveda et al. stated that the productivity of salinated water was influenced by both the temperature of the seawater in the chamber and the temperature outside the glass partition [24]. This physical phenomenon was intricately linked to the process of condensation. Moreover, the vapor within the testing chamber would undergo condensation on the glass partition as a result of the temperature disparity between the inside and outside of the chamber [33]. When evaluating using Figure 8, it was seen that the highest productivity of 267 mL in Chamber 2 occurred at a temperature difference (Δ(Tw-Tog)) of 16.64°C, which was the most significant difference in temperature in Figure 8. This condition is in line with previous studies [25]. The research sequence, illustrated in Figures 8(c), 8(d), and 8(a), establishes a correlation between the temperature difference and the hourly productivity of each chamber.

The assumption was made that fins of varying heights have comparable capacity to absorb the entering heat, based on the average radiation intensity. Prior studies have indicated that the fin configuration influences convective heat transfer, which is closely related to the available internal temperature [23]. The internal temperature has a substantial impact on the production of solar stills. At midday, the fin temperature reached its highest point. The internal temperature influenced the productivity of the solar still. At midday, the temperature of the HCF reached its highest point. A direct proportionality exists between HCF temperature and hourly distillate production. A correlation between T_f and hourly production was illustrated in Figure 9, which was used for comparison. Despite Chamber 2 having a higher productivity value compared to Chambers 3 and 4, the reported T_f falls in between the two. This phenomenon occurred because Chamber 2, which contains a 20 mm HCF, has a height that is directly proportionate to the water level, leading to a relatively low temperature. However, at 16.00. T_f, the temperature of the 20 mm HCF chamber was higher than that of the previously superior 60 mm chambers. As a result of the significant amount of water exposure on the 20 mm HCF surface, the T_f lowers more consistently at 16.00. in comparison to the other chambers. Between the hours of 16.00. and 18.00., the 20 mm HCF chamber had a higher hourly production rate of 83 mL compared to 77 mL and 44 mL in the 40 mm and 60 mm HCF

chambers, respectively. The zone where heat is released in this HCF is commonly referred to as the discharge zone. The decrease in T_f at 60 mm HCF is a result of the tremendous convective heat transfer process from the unexposed fin surface area from seawater to the inside air.

still is mostly influenced by the maximum absorption of radiation intensity by the absorber fin.

3.3 CS4 productivity

The study used the productivity of distilled water as a crucial measure to evaluate the effectiveness of increasing the fin height. Furthermore, Figure 10 illustrates the five-day evaluation of distilled production. The data indicated that the maximum productivity of each chamber reached its highest point at different times. Chamber 1 reached its peak on the second day with a volume of 1075 mL, while Chamber 2 reached its peak on the fifth day with a volume of 2115 mL. The maximum output achieved by Chamber 3 was 1490 mL on day 5, while Chamber 4 produced a total of 1055 on the third day. The daily acquisition process was affected by diverse fluctuations in radiation intensity that entered the system. Regarding the height of the fin, as mentioned in Figure 10, there are additional significant parameters that have an impact. According to Shadi et al. [34] the production of solar

Figure 9. The relationship between the plotted T_f and the hourly productivity of each testing chamber

(a) Chamber 1

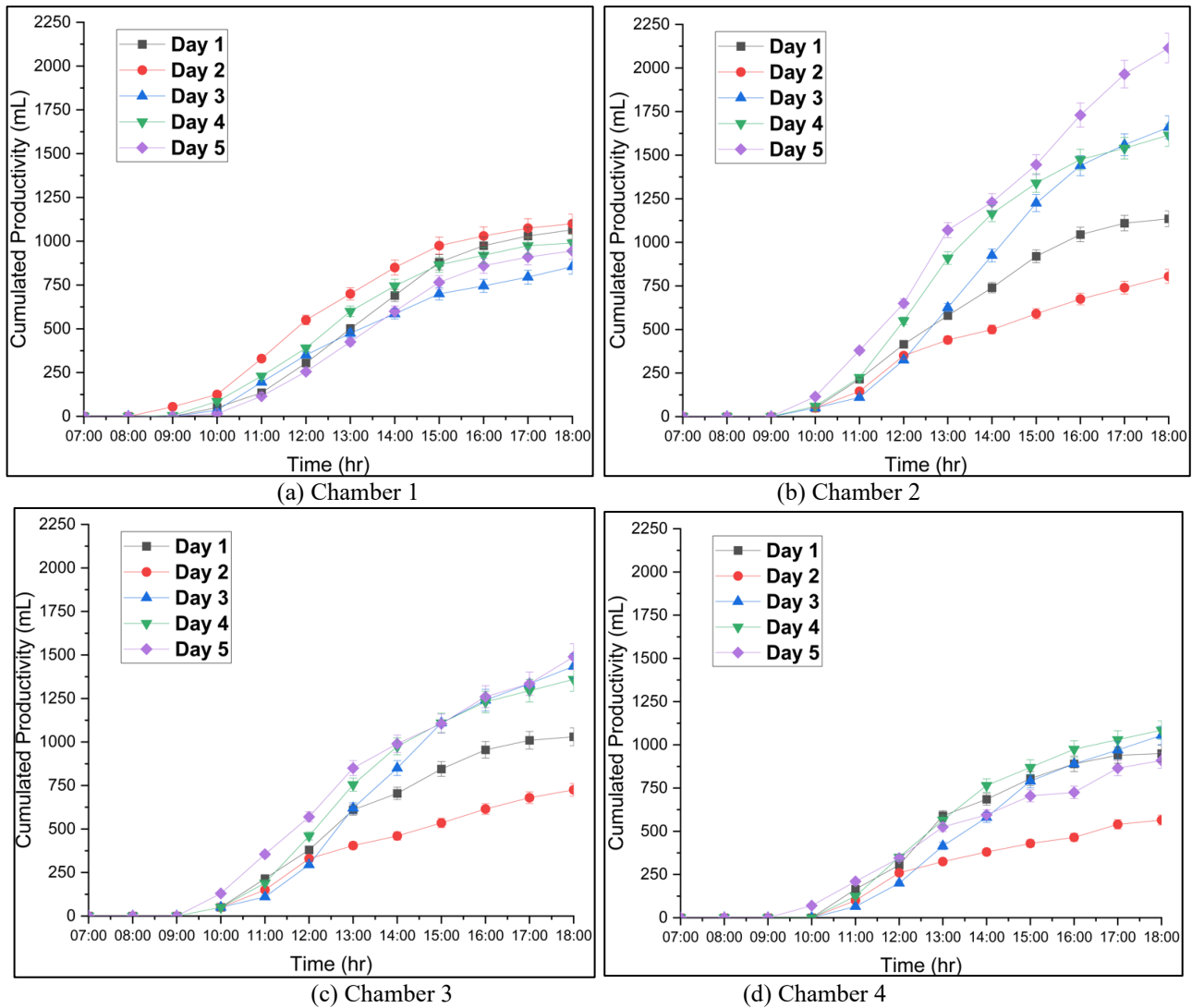(b) Chamber 2

(c) Chamber 3

(d) Chamber 4

Figure 10. Total daily productivity of each testing chamber

450

Figure 11 displays the average daily productivity results for each chamber. The highest accumulated production was gained by Chamber 2 with 1466 mL. The cumulative productivity of seawater decreases as the height of the fin increases. The production decreased from Chamber 2, which had a volume of 1466 mL, to Chamber 3, which had a volume of 1208 mL, and then from Chamber 3 to Chamber 4, which had a volume of 913 mL. On the contrary, a clear trendline became apparent between Chamber 1 and Chamber 2. The cumulated production increased from 986 mL to 1466 mL. This increased production aligns with previous research as a result of the implementation of fins and the consequent improvement in convective heat absorption [11, 15, 35]. The data indicated a specific increase in productivity of 48.68% when comparing a conventional CS4 with a 20 mm in height. Based on the test results, the production of distilled water showed a progressive decline as the fin height increased, which is in line with the result of Qiu et al.'s research [36]. However, this is in contrast with El-Sebaii et al., who asserted that there was an increase in freshwater production as the fin height increased [21]. The systems did not fully absorb the entered energy; the top surface fin experienced a higher temperature, but it was not in direct contact with seawater.

Moreover, the presence of taller fins distracted the convective heat transfer within the chamber. The absorbed energies were not efficiently dissipating by evaporation, resulting in reduced productivity in Chamber 3 and 4 compared to Chamber 2 productions gained. Even Chamber 4 productivity was lower than conventional Chamber 1.
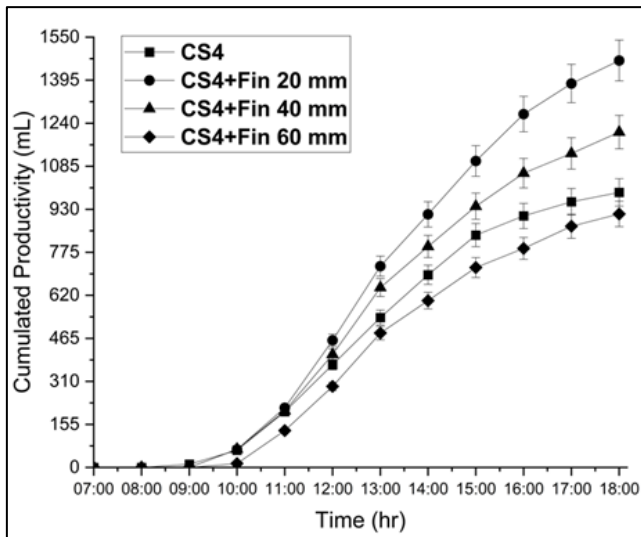

Figure 11. Total productivity in each testing chamber during the day of the experiments
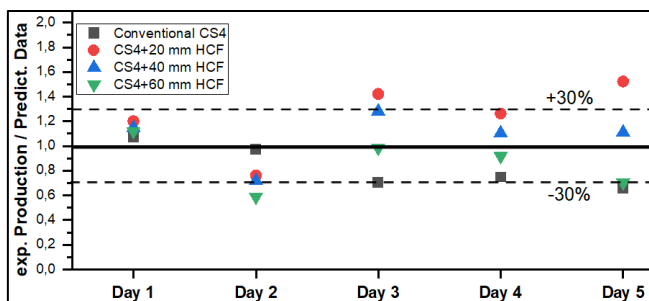

Figure 12. Comparison of the predicted data with the existing experimental productivity data

The productivity data collected during the day experiment was analyzed using least squares regression and RMSE Eq. (6). The key component considered was the height of the HCF, whereas the confounding variable was the solar intensity, which varied each day. Figure 12 shows an evenly distributed comparison between the experimental and predicted data, with a margin of error of around ± 30%. The proximity between the residual plot and the regression line in Figure 13 demonstrates the adherence of the residuals from the regression analysis on the experimental and predicted data to a normal distribution. This suggests that the results of the experiment are statistically similar. Previous studies, similar to this distribution analysis, carried out statistical analyses of the same distribution [12, 26].
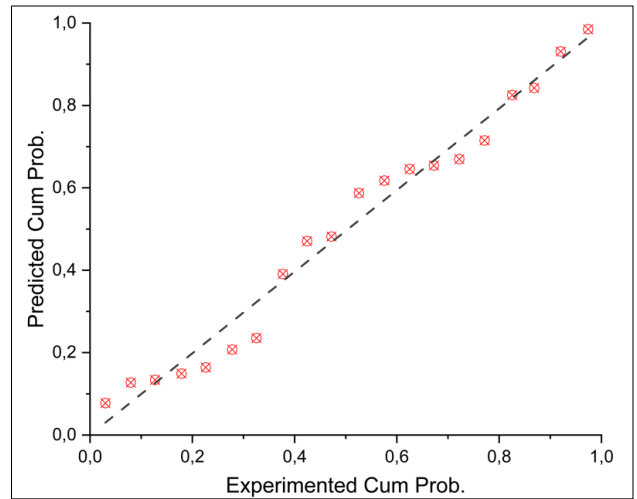

Figure 13. Residual plot normal distribution standardized
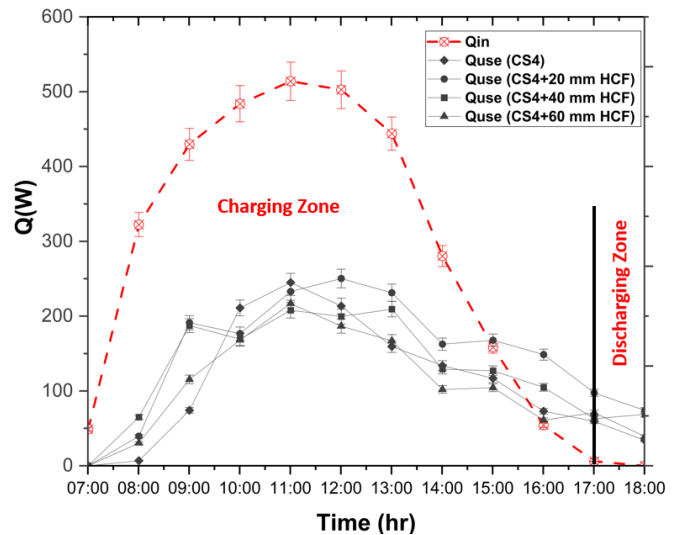

Figure 14. The graph of average Qin and Quse

Figure 14 depicts the calculation of input energy and energy consumption for each CS4 chamber. The energy entering the system was calculated using Eq. (7), yielding an average total of 3243.65 W. The desalination system did not adequately capture and utilize the energy that is supplied to the chamber responsible for evaporating seawater. The Quse values employed for the evaporation process in Chambers 1-4 are as follows: 994.77 W, 1328.91 W, 1148.15 W, and 946.11 W, as stated in Equation 8. Consequently, each chamber attained efficiencies of 30.66%, 40.96%, 35.39%, and 29.16% accordingly, as shown in Figure 15. Chamber 2, which has a

20 mm implementation, has the highest level of efficiency. The fundamental configuration involves the mass of water, which ensures a consistent water level in the basin. The height of the CS4+20 mm HCF is approximately proportional to the height of the water in the chamber. The proportional height between the fin and the water is suitable because all surfaces of the 20 mm HCF make contact with seawater. Therefore, the transmission of heat from the fin to the saltwater may be more effective in terms of absorbed energy. Distinct trendlines are observed in Chamber 3 (40 mm HCF) and Chamber 4 (60 mm HCF), where some of the HCF area is not in direct contact with water. As a result, the exposed fin area in the chamber experienced a loss of energy, dissipating through the internal air to partition glass and releasing it to the surroundings. This statement refers to a prior study that found that energy loss happens between the seawater and internal air, which then spreads through convection to the glass partition before being released into the environment through conduction and radiation [37].

This study evaluated the amount of energy loss to the environment through the partition glass and CS4 wall by utilizing Eqs. (16), (17), and (18). The energy dissipated by radiation and convection through the partition glass accounts for 55.52% (Chamber 1), 48.89% (Chamber 2), 39.85% (Chamber 3), and 42.38% (Chamber 4) of the total average energy entering the system. The energy released by conduction and convention processes through the side and bottom walls of the chamber accounts for 13.80%, 10.03%, 24.75%, and 28.44% of the total incoming energy, respectively, for chambers 1 to 4. Table 4 presents a comparative analysis between this research and previous studies.
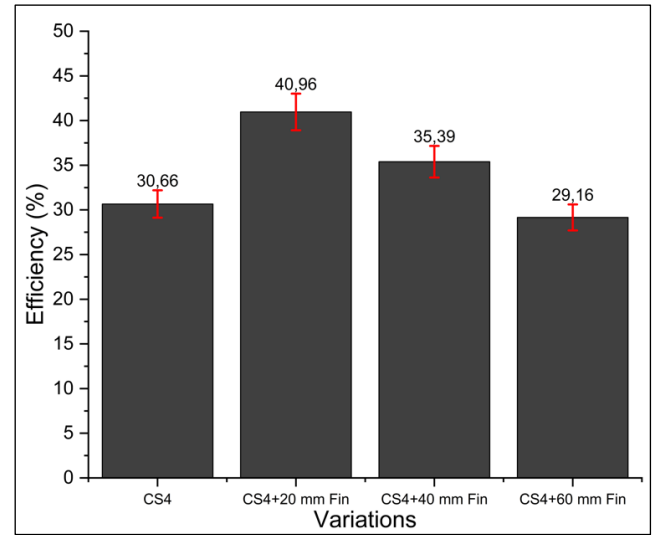

Figure 15. The resulting efficiency in each solar still chamber

Table 4. Comparative analysis of the current study and previous study

Ref.	Type of Solar Still	Variation	Concluding
[19]	Hemispherical Solar Still (0.11 m^2 absorber area) Operates on: April	Iron cylindrical fin 10, 20, 30 mm)	Using fin height modifications, productivity increases in the 70 mm fin spacing configuration by 39.21%, 56.37%, and 52.45% for 10 mm, 20 mm, and 20 mm iron fins, respectively.
[1]	Single-Slope Solar Still (1 m^2 absorber area) Operates on: August	10, 20, 30, and 40 mm FLBS Fin	As the fin height increases, there is a continuous and noticeable improvement in productivity and efficiency. The 40 mm fin has the highest level of production, which also experiences a 13.7 % increase.
Present Study	Single-Slope Solar Still (0.735 m^2 absorber area) Operates on: June	Experimental analysis with heights of 0, 20, 40, and 60 mm hollow circular fin	Efficiency decreases by 40.96%, 35.39%, and 29.16% as fin height increases. As the HCF surface becomes more exposed, it absorbs more heat, which convection then releases and expels through the partition glass.

4. CONCLUSION

The experimental examination of the utilization of various heights of circular fins in single-slope solar still desalination was satisfactorily completed. The discussion section provides a detailed elucidation of the operational performance of each solar still. This research yields the following conclusions:

a) Increased fin height results in decreased productivity and efficiency in solar stills. The efficiency percentages and total production volumes for 20 mm, 40 mm, and 60 mm HCF were 40.96% (1466 mL), 35.39% (1208 mL), and 29.16% (913 mL), respectively.

b) The implementation of a 20 mm HCF increased productivity and efficiency from conventional solar stills to CS4 by 486 mL and 10.30%, respectively.

c) The solar still partition glass emits energy to the environment at rates of 55.52%, 48.89%, 39.85%, and 42.38% for conventional 20 mm, 40 mm, and 60 mm HCF systems.

d) The energy loss through the bottom and side walls accounted for 13.80%, 10.03%, 24.75%, and 28.44% of the energy entering the system from standard CS4, 20 mm HCF, 40 mm HCF, and 60 mm HCF, respectively.

e) The experimental data exhibits a significant correlation and distribution, with a projected distribution range of ± 30% and residual data distributed normally.

REFERENCES

[1] El-Sebaii, A.A., Ramadan, M.R.I., Aboul-Enein, S., El-Naggar, M. (2015). Effect of fin configuration

parameters on single basin solar still performance. Desalination, 365: 15-24. https://doi.org/10.1016/j.desal.2015.02.002

[2] Agrawal, A., Rana, R.S., Srivastava, P.K. (2017). Resource-efficient technologies heat transfer coefficients and productivity of a single slope single basin solar still in Indian climatic condition: Experimental and theoretical comparison. Resource-Efficient Technologies, 3(4): 466-482. https://doi.org/10.1016/j.reffit.2017.05.003

[3] Gude, V.G. (2016). Desalination and sustainability-An appraisal and current perspective. Water Research, 89: 87-106. https://doi.org/10.1016/j.watres.2015.11.012

[4] Schiffier, M. (2004). Perspectives and challenges for desalination in the 21st century, Desalination, 165: 1-9. https://doi.org/10.1016/j.desal.2004.06.001

[5] Somanchi, N.S., Sagi, S.L.S., Kumar, T.A., Kakarlamudi, S.P.D., Parik, A. (2015). Modelling and analysis of single slope solar still at different water depth. Aquatic Procedia, 4: 1477-1482. https://doi.org/10.1016/j.aqpro.2015.02.191

[6] Abyar, H.S (2007). A review of desalination by solar still. In Solar Desalination for the 21st Century, Springer, Dordrecht, pp. 207-214. http://doi.org/10.1007/978-1-4020-5508-9_15

[7] Baharin, Z.A.K., Mohammad, M.H. (2018). Experimental investigations on the effects of design parameters on single slope solar still evaporation rate under Malaysian conditions. Journal of Mechanical Engineering, 5(6): 16-24.

[8] Tiwari, G.N., Sahota, L. (2017). Review on the energy and economic efficiencies of passive and active solar distillation systems. Desalination, 401: 151-179. https://doi.org/10.1016/j.desal.2016.08.023

[9] Katekar, V.P., Deshmukh, S.S. (2020). A review of the use of phase change materials on performance of solar stills. Journal of Energy Storage, 30: 101398. https://doi.org/10.1016/j.est.2020.101398

[10] Rajaseenivasan, T., Srithar, K. (2016). Performance investigation on solar still with circular and square fins in basin with CO_2 mitigation and economic analysis. Desalination, 380: 66-74. https://doi.org/10.1016/j.desal.2015.11.025

[11] Jani, H.K., Modi, K.V. (2019). Experimental performance evaluation of single basin dual slope solar still with circular and square cross-sectional hollow fins. Solar Energy, 179: 186-194. https://doi.org/10.1016/j.solener.2018.12.054

[12] Septiyanto, M.D., Sasongko, F.A., Hadi, S., Budiana, E.P. (2023). The using hollow circular fin absorber on the performance of single slope solar still. Lecturer Notes in Mechanical Engineering, 5-8. https://doi.org/10.1007/978-981-97-0106-3

[13] Mirmanto, Sayoga, I.M.A., Wijayanta, A.T., Sasmito, A.P., Aziz, M. (2021). Enhancement of continuous-feed low-cost solar distiller: Effects of various fin designs. Energies, 14(16): 4844. https://doi.org/10.3390/en14164844

[14] Abdelgaied, M., Harby, K., Eisa, A. (2021). Performance improvement of modified tubular solar still by employing vertical and inclined pin fins and external condenser: An experimental study. Environmental Science and Pollution Research, 28(11): 13504-13514. https://doi.org/10.1007/s11356-020-11585-3

[15] Daliran, A., Ajabshirchi, Y. (2018). Theoretical and experimental research on effect of fins attachment on operating parameters and thermal efficiency of solar air collector. Information Processing in Agriculture, 5(4): 411-421. https://doi.org/10.1016/j.inpa.2018.07.004

[16] Hamzah, F.A., Septiyanto, M.D., Budiana, E.P., Prasetyo, A. (2023). The using of thermal energy storage on single slope solar still distiller. E3S Web of Conferences, 465: 01023. https://doi.org/10.1051/e3sconf/202346501023

[17] Manokar, A.M., Winston, D.P. (2017). Experimental analysis of single basin single slope finned acrylic solar still. Materials Today: Proceedings, 4(8): 7234-7239. https://doi.org/10.1016/j.matpr.2017.07.051

[18] Abdul-Wahab, S.A., Al-Hatmi, Y.Y. (2013). Performance evaluation of an inverted absorber solar still integrated with a refrigeration cycle and an inverted absorber solar still. Energy for Sustainable Development, 17(6): 642-648. https://doi.org/10.1016/j.esd.2013.08.006

[19] Attia, M.E., Kabeel, A.E., Abdelgaied, M., El-Maghlany, W.M., Bellila, A. (2021). Comparative study of hemispherical solar distillers iron-fins. Journal of Cleaner Production, 292: 126071. https://doi.org/10.1016/j.jclepro.2021.126071

[20] El-Sebaii, A.A., Ramadan, M.R.I., Aboul-Enein, S., El-Naggar, M. (2015). Effect of fin configuration parameters on single basin solar still performance. Desalination, 365: 15-24. https://doi.org/10.1016/j.desal.2015.02.002

[21] Psiloglou, B.E., Santamouris, M., Asimakopoulos, D.N. (1994). On the atmospheric water vapor transmission function for solar radiation models. Solar Energy, 53(5): 445-453. https://doi.org/10.1016/0038-092X(94)90059-0

[22] Omara, Z.M., Hamed, M.H., Kabeel, A.E. (2011). Performance of finned and corrugated absorbers solar stills under Egyptian conditions. Desalination, 277(1-3): 281-287. https://doi.org/10.1016/j.desal.2011.04.042

[23] Sharshir, S.W., Kabeel, A.E., Elsheikh, A.H., Peng, G. (2017). Thermal performance and exergy analysis of solar stills – A review. Renewable and Sustainable Energy Reviews, 73: 521-544. https://doi.org/10.1016/j.rser.2017.01.156

[24] Mevada, D., Panchal, H., Israr, M. (2020). Groundwater for sustainable development effect of fin configuration parameters on performance of solar still: A review. Groundwater for Sustainable Development, 10: 100289. https://doi.org/10.1016/j.gsd.2019.100289

[25] Velmurugan, V., Gopalakrishnan, M., Raghu, R., Srithar, K. (2008). Single basin solar still with fin for enhancing productivity. Energy Conversion and Management, 49(10): 2602-2608. https://doi.org/10.1016/j.enconman.2008.05.010

[26] Radomska, E., Mika, Ł. (2023). Long-term modeling of the performance of a solar still with phase-change material. Applied Thermal Engineering, 235: 121339. https://doi.org/10.1016/j.applthermaleng.2023.121339

[27] Alaian, W.M., Elnegiry, E.A., Hamed, A.M. (2016). Experimental investigation on the performance of solar still augmented with pin-finned wick. Desalination, 379: 10-15. https://doi.org/10.1016/j.desal.2015.10.010

[28] Yousef, M.S., Hassan, H., Kodama, S., Sekiguchi, H. (2019). An experimental study on the performance of single slope solar still integrated with a PCM-based pin-

finned heat sin. Energy Procedia, 156: 100-104. https://doi.org/10.1016/j.egypro.2018.11.102

[29] Jahanpanah, M., Sadatinejad, S.J., Kasaeian, A., Jahangir, M.H., Sarrafha, H. (2021). Experimental investigation of the effects of low-temperature phase change material on single-slope solar still. Desalination, 499: 114799. https://doi.org/10.1016/j.desal.2020.114799

[30] Sachan, V., Rai, A.K. (2016). Studies on finned basin solar still. International Journal of Mechanical Engineering and Technology, 7(3): 119-124.

[31] Ranjan, K.R., Kaushik, S.C. (2013). Energy, exergy and thermo-economic analysis of solar distillation systems: A review. Renewable and Sustainable Energy Reviews, 27: 709-723. https://doi.org/10.1016/j.rser.2013.07.025

[32] Al-Hamadani, A.A.F., Shukla, S.K. (2016). Experimental investigation and thermodynamic performance analysis of a solar distillation system with PCM storage: Energy and exergy analysis experimental investigation and thermodynamic performance analysis of a solar distillation system with PCM storage: Energy and exergy analysis. Distributed Generation & Alternative Energy Journal, 29(4): 7-24. https://doi.org/10.1080/21563306.2014.11442728

[33] Prakash, P., Velmunurugan, V. (2015). Effect of wind speed and water depth on the performance of a solar still. Journal of Chemical and Pharmaceutical Sciences, 7: 12-14.

[34] Shadi, M., Abujazar, S., Fatihah, S., Rakmi, A.R., Shahrom, M.Z. (2016). The effects of design parameters on productivity performance of a solar still for seawater desalination: A review. Desalination, 385: 178-193. https://doi.org/10.1016/j.desal.2016.02.025

[35] Rabhi, K., Nciri, R., Nasri, F., Ali, C., Bacha, H.B. (2017). Experimental performance analysis of a modified single-basin single-slope solar still with pin fins absorber and condenser. Desalination, 416: 86-93. https://doi.org/10.1016/j.desal.2017.04.023

[36] Qiu, G., Sun, J., Ma, Y., Qu, J., Cai, W. (2018). Theoretical study on the heat transfer characteristics of a plain fin in the finned-tube evaporator assisted by solar energy. International Journal of Heat and Mass Transfer, 127: 847-855. https://doi.org/10.1016/j.ijheatmasstransfer.2018.07.106

[37] Panchal, H. (2016). Performance investigation on variations of glass cover thickness on solar still: experimental and theoretical analysis. Technology and Economics of Smart Grids and Sustainable Energy, 1(1): 7. https://doi.org/10.1007/s40866-016-0007-0